# Real-Time 3-Dimensional Echocardiography Provides New Insight Into Mechanisms of Tricuspid Valve Regurgitation in Patients With Hypoplastic Left Heart Syndrome

K. Takahashi, MD; A. Inage, MD; I. M. Rebeyka, MD; D. B. Ross, MD; R. B. Thompson, PhD; A. S. Mackie, MD; J. F. Smallhorn, MBBS

***Background***—Tricuspid regurgitation in hypoplastic left heart syndrome has an impact on outcome, but its mechanisms remain unclear.

***Methods and Results***—Real-time 3-dimensional echocardiography was performed in 35 patients with hypoplastic left heart syndrome (age, 1 month to 10 years; 10 after first-stage Norwood, 12 after superior cavopulmonary shunt, 13 after Fontan). From the 3-dimensional data set, we marked the annulus in systole and diastole. At mid systole, we marked the location of the papillary muscle tip and point of chordal attachment to the leaflet. We traced the surfaces of the tricuspid valve leaflets and measured the volume of leaflet prolapse, tethering, annular and septal leaflet areas, and papillary muscle position. Seventeen patients had moderate tricuspid regurgitation (prolapse, 7; tethered leaflets, 7) and 18 mild (prolapse, 0; tethered leaflets, 7). Multiple linear regression analysis revealed that moderate tricuspid regurgitation is associated with leaflet tethering and prolapse; that in hypoplastic left heart syndrome with tethered leaflets, the papillary muscle is displaced laterally and the tricuspid annulus is more planar; and that enlargement of the annulus at mid systole, small septal leaflet area, and age affect the degree of prolapse.

***Conclusion***—In hypoplastic left heart syndrome, moderate tricuspid regurgitation may be associated with increasing age, geometrical changes of the annulus, leaflet prolapse, lateral papillary muscle displacement, and subsequent leaflet tethering, as well as a smaller septal leaflet. **(*Circulation*. 2009;120:1091-1098.)**

**Key Words:** echocardiography ■ heart defects, congenital ■ pediatrics ■ surgery



In hypoplastic left heart syndrome (HLHS), significant tricuspid regurgitation (TR)[1,2] occurs at a frequency of 8.5% to 16%.[3,4] In general, TR may be due to dilatation of the right ventricle (RV), RV geometrical change, left ventricle (LV)–RV interaction, RV dysfunction, and intrinsic abnormalities of the leaflets and supporting apparatus.[1–4] Several studies have attempted to address risk factors for the development of TR[2–5] but have provided little insight.

**Clinical Perspective on p 1098**

Tricuspid valve (TV) tethering resulting from geometrical change of the RV and abnormalities of annular function are important mechanisms of functional TR.[6–9] Using real-time 3-dimensional echocardiography (RT3D), we previously demonstrated the importance of mitral-tricuspid annular interaction[10] and the role of tricuspid annular function and papillary muscle (PM) displacement as a cause of TR in HLHS.[11] Our hypothesis was that abnormalities of tricuspid annular function and PM location are directly related to the severity of TR in HLHS through disturbances of leaflet function.

## Methods

### Patient Characteristics

Between January 2006 and November 2007, we acquired consecutive 2-dimensional (2D) and RT3D images in patients with HLHS beyond their first-stage Norwood procedure. The patients were recruited as they came to the echocardiography laboratory for routine studies. We also collected data from normal subjects for comparison. Patients with qualitatively preserved RV function and normal sinus rhythm were included. Patients with atrioventricular septal defect or significant TR before their first-stage Norwood were excluded. The protocol was approved by the University of Alberta Ethics Committee.

### Two-Dimensional Echocardiography

We performed 2D echocardiography using an IE33 with an S4, S8, or S12 transducer (Philips Medical Systems, Bothwell, Wash). The degree of TR was assessed by 2D vena contracta (VC) width[12] at the orifice and then divided into 2 groups. TR was characterized on a 0 to 4+ grading scale and defined as follows: 0=none, 1=mild (narrow regurgitant jet, <2 mm, single jet), 2=mild to moderate (jet <4 mm, multiple jets, or both; mild atrial enlargement), 3=moderate to severe (wide jet >4 mm that reaches the back wall of the atrium; moderate atrial enlargement), and 4=severe (wide jet >4 mm that reaches the back wall of the atrium; reversal of flow in the hepatic veins; severe atrial enlargement).[2,11] Studies with TR in the range of

Received July 23, 2008; accepted June 19, 2009.

From the Departments of Pediatrics, Surgery and Biomedical Engineering, University of Alberta, and Stollery Children's Hospital Edmonton, Alberta, Canada.

Correspondence to Jeffrey F. Smallhorn, MBBS, University of Alberta Hospital, Room 4C2, Walter C. Mackenzie Health Sciences Centre, Edmonton, Alberta, T6G 2B7, Canada. E-mail jeffrey.smallhorn@capitalhealth.ca



*Circulation* **is available at http://circ.ahajournals.org** **DOI: 10.1161/CIRCULATIONAHA.108.809566**

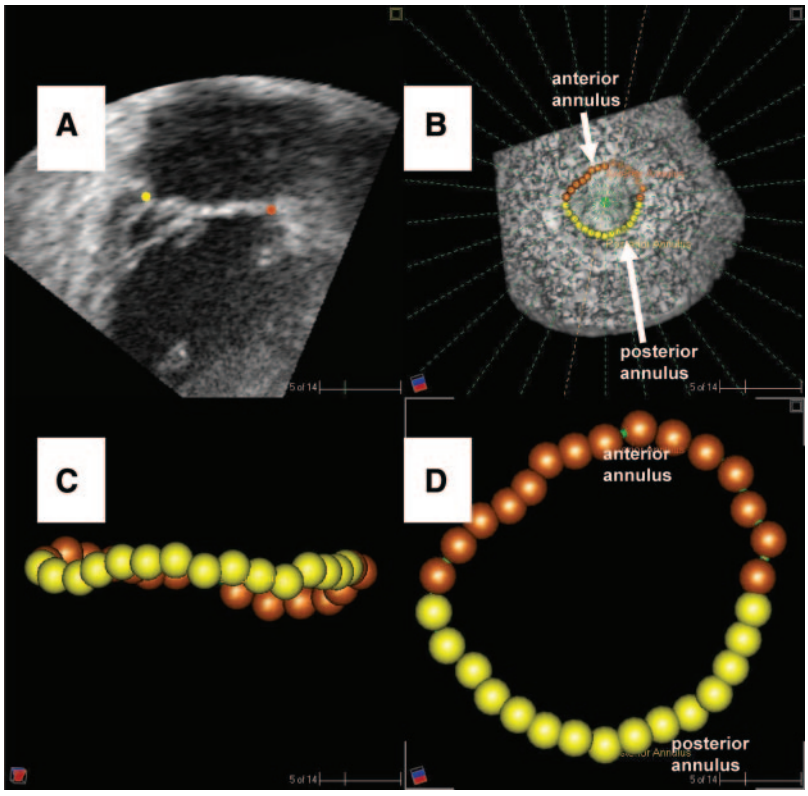


**Figure 1.** Three-dimensional tricuspid annulus reconstruction. Annulus in each plane is marked with points (A), resulting in 3D annulus reconstruction. (B, C, and D).



0 to 2 were characterized as mild, whereas those with grade 3 to 4 were characterized as moderate. RV function was assessed by fractional area change in the apical 4-chamber view. The RV long-axis, maximal minor-axis (S1), and mid minor-axis (S2) dimensions were measured as previously described.[13] The ratio of RV minor-axis dimension to long-axis dimension was calculated for both S1 and S2 (sphericity index) as an index of RV asymmetry.[13] The relationship of the degree of TR to LV size was assessed by measuring the ratios of LV to RV length at end diastole and the mitral valve to TV annular size.

## Volumetric Image Acquisition

Three-dimensional images were obtained with an RT3D system (IE33, Philips Medical Systems) equipped with a Matrix X3–1 or X7–2 probe. For all patients, full-volume images of the TV and supporting apparatus were obtained from the apex, including color Doppler data. Data were transferred to a personal computer for offline analysis.

## Measurements of VC Area by 3D

Cropping of the RT3D color data set was performed in the 4-chamber view to measure VC area[14] with CardioView software (TomTec Inc, Munich, Germany). When >1 VC was present, the areas were summed.

## Tricuspid Morphological Reconstruction

With TomTec, data were acquired by obtaining 15 slices around the line penetrating the center of the tricuspid annulus (every 20°) at end diastole and mid systole (Figure 1). End diastole was the frame just before aortic valve opening, and end systole was the frame of valve closure. Mid systole was determined by counting the total systolic frames and choosing the midpoint between them. On each 2D plane from the 3D data set, we placed a marker on the annular hinge points (Figure 1). Second, from the 3D data set, we obtained seven 2D planes that passed through the midpoint of the septum at the annular level (Figure 2). This divided the TV and its apparatus into 7 segments. On these 2D planes at mid systole, we placed markers on the anterior and posterior leaflets at their points of coaptation with the septal leaflet to measure the septal leaflet area (Figure 2). The angle between each 2D plane was 15°. On each 2D plane, we placed 7 markers on the tricuspid leaflets for subsequent graphical 3D reconstruction (Figure 2). Next, we found the 2D plane from the 3D data set that passed the midpoint of the septum and included the tip of the anterior or posterior PM. We marked a point on the tip of the

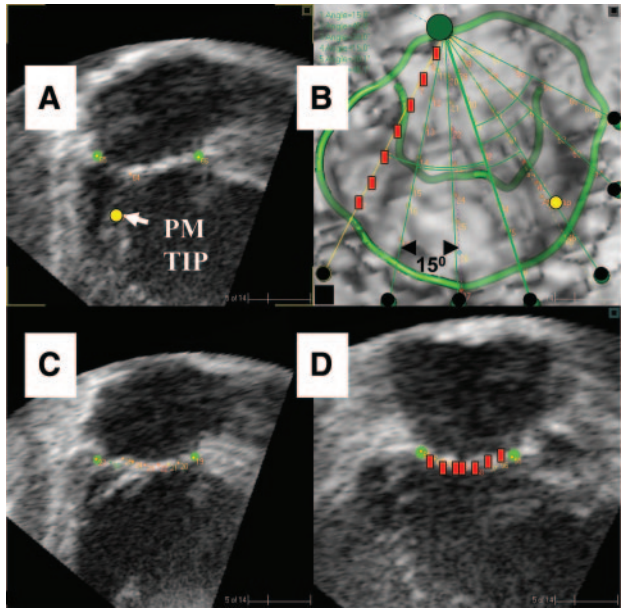


**Figure 2.** Three-dimensional tricuspid leaflet reconstruction. The annulus and the leaflets were marked with points on each plane (small green dots on 2D images; A, C, and D). The points of coaptation of the septal and combined anterior and posterior leaflets were noted (B; inner green semicircle). Next, 7 planes were obtained separated by 15° (B; large green dot). After this, 7 dots were placed on the leaflets in each plane (B and D; red squares). The planes that passed the anterior (A) and posterior PM were identified. We marked the point on the tip of the PM (A and B; yellow dot).

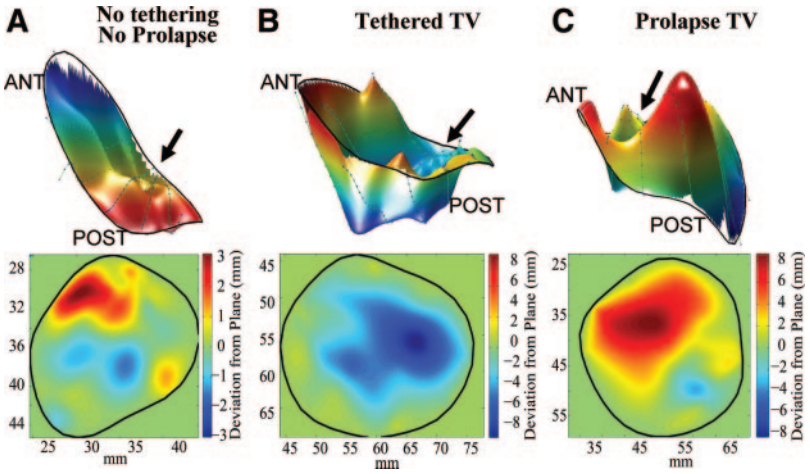


**Figure 3.** Visualization of tricuspid leaflet geometry in HLHS reconstructed with customized software without tethering/prolapse (A), with tethering (B), and with prolapse leaflets (C). The blue area represents the region below the least-fit annular plane (close to the apex). The red area represents the region above the least-fit annular plane (toward the atrium). The dots on the images represent the actual valve data points obtained from the TomTec software that have been mathematically interpolated on MatLab to smooth the image. The black arrows shows the location of the septal leaflet. Note that the main area of prolapse (C) involves the midportion of the anteroposterior leaflets indicated by red. ANT indicates anterior; POST, posterior.

PMs and the point where the chordae attached to leaflets (Figure 2). All points were converted into spatial coordinates (x, y, and z) and exported to customized MatLab-based software (MathWorks Inc, Natick, Mass) for reconstruction. This propriety software was used to develop 3D models of the TV and its apparatus for analysis.

## Measurements of 3D Echocardiographic Data

### *Annular Area and Perimeter*

Annular area was calculated as the sum of 30 small triangles composed of 2 adjacent annular points and a mathematically calculated gravity center of the annulus. The annular perimeter was calculated as the sum of the point-point distance traversing 30 points on annulus. The annular area and perimeter were indexed to body surface area (BSA). The percent of area change at mid systole was calculated as follows: area at end diastole−area at mid systole/area at end diastole×100.

### *Ratios of Anterior-Posterior to Left-Right Diameter and Septal Leaflet to TV Area*

From an enface view, the program demonstrated the annular and coaptation line between the septal and anterior-posterior leaflets (Figure 2B). We manually measured the diameter of the TV annulus in the anterior-posterior, left-right direction. The ratio of septal leaflet to TV area was measured by navigating through the individual 2D slices in the 3D data set and placing markers on the leaflets, which accommodated their various undulations (Figure 2D). The previously identified closure line between the septal and anterior-posterior leaflets was used to separate the septal leaflet from the total area of the TV. The ratio of anterior-posterior to left-right diameter was calculated as the anterior-posterior diameter divided by the left-right diameter. The ratio of septal leaflet to TV area was calculated as septal leaflet area divided by tricuspid annular area.

### *Measurements of Prolapse and Tethering Volume*

For quantitative analysis, the TV annular plane was determined on the basis of a saddle-like annular shape in each subject.[10] We measured the volume enclosed between the annular plane and the tricuspid leaflets. This tethered and/or prolapse volume was indexed to BSA (Figure 3).

### *Measurements of Annular Position*

The anatomic locations of the high (toward the right atrium) and low (toward the RV) annular points relative to the best-fit (nonnegative least-squares) plane were plotted as a function of annular position from the reconstruction of the annulus (Figure 4). Radial angle represents the position of the annulus; 0° is the mid point of the septum, and the degree increased with clockwise rotation when the TV was viewed from above. In all cases, 2 positive peaks were observed at the anterior and posterior positions of the tricuspid annulus, and 2 negative peaks were seen at the lateral and septal positions (Figure 4). The height of all 4 points from the least-squares fit plane was measured. The degree of nonplanarity was measured by the distance between the high and low points calculated as follows: mean height=(the height at anterior+height at posterior−height at septal−height at lateral)/2. These measurements were indexed to RV length.

### *Bending Angle of the Tricuspid Annulus*

The TV annulus was divided into anterior and posterior sections, as defined by the bending points A and C (Figure 4). A best-fit (nonnegative least-squares) plane was fit to the annular points in each of the 2 sections (Figure 4, bottom), from which the bending angle was determined as the angle between the normal lines for each plane.

### *PM Angle*

Figure 5 illustrates the method used to calculate the angle between the annulus and the PMs. The angle was determined from the best-fit plane of the tricuspid annulus.

## Statistical Analysis

Continuous variables are presented as median (range) or mean±SD as appropriate. Differences among groups of continuous valuables

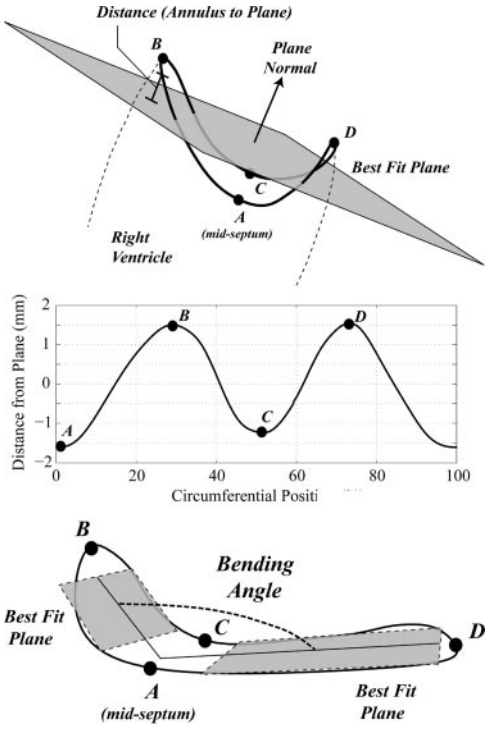


**Figure 4.** Diagram demonstrating the vertical geometry of the TV from mathematically derived best-fit plane. A, The low point at midseptum; B, the anterior high point; C, the lateral low point; and D, the posterior high point.

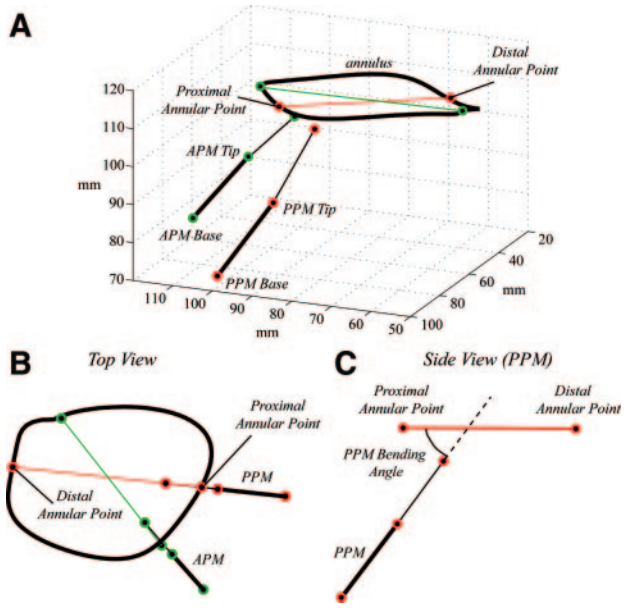


**Figure 5.** Schematic demonstrating the angle measured between the tricuspid annulus and the PMs, as seen from above, from the side, and in a 3D format. APM indicates anterior PM; PPM, posterior PM.

were determined by 1-way ANOVA with Scheffe multiple-comparisons procedure. Pearson product-moment correlation coefficient was used to determine the strength of the relationship between continuous variables. Multiple linear regression analysis was performed with backward variable selection. Variables were included in the initial model if $P<0.10$ on univariate analysis. Statistical significance was set at $P<0.05$. Analyses were performed with commercially available statistical software (Stata version 9, Stata Corp, College Station, Tex).

# Results

## Participant Characteristics and 2D Echocardiographic Measurements

This study included 39 consecutive patients with HLHS, of whom 4 were excluded for a poor ultrasound window. The remaining 35 had a median age of 3.3 years (range, 1 month to 10.8 years); the 17 healthy volunteers had a median age of 5.4 years (range, 6 months to 10.8 years). Ten previously underwent only a Norwood/Sano procedure (RV–pulmonary artery conduit), 12 had a bidirectional cavopulmonary shunt, and 13 had a Fontan. For both patients and control subjects, the median frame rate of the RT3D data sets was 42 Hz (range, 22 to 69 Hz).

## RV Sphericity Index

There was some difference in RV sphericity index between patients and control subjects but not between patient groups (Table 1).

## Rationale for Subcategories

There was a normal TV mean tethering volume of 0.47±0.22 mL/m$^2$ in control subjects. Therefore, abnormal TV tethering was defined as a tethering volume of ≥0.69 mL/m$^2$. In control subjects, the ratio of TV prolapse volume to BSA was only 0.01±0.02 mL/m$^2$. If a cutoff for prolapse volume of 0.03 mL/m$^2$ was used to define significant prolapse, then except for the 12 patients with tethering, almost all the patients had some degree of prolapse compared with control subjects. To identify those patients in whom significant prolapse might be of importance as a mechanism of TR, we used the mean prolapse volume of all those who had no tethering as the cutoff to define significant prolapse (>0.46 mL/m$^2$).

With these criteria, 16 patients, 13 with mild TR and 3 with moderate TR, were classified as group N. The 7 patients

**Table 1. Patients Characteristics and 2D Echocardiographic Measurements**

| | Control Subjects (Group C) | HLHS, No Tethering/Prolapse (Group N) | HLHS, Tethered Valve (Group T) | HLHS, Prolapsed Valve (Group P) | *P* |
|---|---|---|---|---|---|
| n (male) | 17 (10) | 16 (11) | 12 (9) | 7 (6) | |
| Age, y | 5.4±2.5 | 3.4±3.0 | 2.0±1.9 | 5.3±4.5 | C vs T* |
| BSA, m$^2$ | 0.75±0.18 | 0.57±0.22 | 0.47±0.18 | 0.70±0.36 | C vs T* |
| Stage of Norwood, n | | | | | |
| 1 | | 5 | 4 | 1 | |
| 2 | | 7 | 3 | 2 | |
| 3 | | 4 | 5 | 4 | |
| TR class, n | | | | | |
| Mild | | 13 | 5 | 0 | |
| Moderate | | 3 | 7 | 7 | |
| 2D VC width, mm | | 0.23±0.2 | 0.38±0.19 | 0.58±0.12 | N vs P‡ |
| 2D VCA calculated by 2D, mm$^2$ | | 0.07±0.11 | 0.14±0.10 | 0.28±0.12 | N vs P,‡ P vs T* |
| MV diameter *z* score | | −11.0±4.3 | −13.0±6.2 | −10.7±4 | 0.15 |
| RV fractional area change, % | 37.8±6.7 | 34.4±11.3 | 31.1±7.3 | 42.3±9.6 | 0.05 |
| S1/L ratio at ED | 0.64±0.12 | 0.73±0.18 | 0.87±0.18 | 0.75±0.22 | C vs T† |
| S1/L ratio at MS | 0.66±0.14 | 0.76±0.2 | 0.84±0.2 | 0.75±0.18 | 0.08 |
| S2/L ratio at ED | 0.45±0.08 | 0.68±0.17 | 0.77±0.15 | 0.65±0.18 | C vs N,‡ C vs T,‡ C vs P* |
| S2/L ratio at MS | 0.46±0.13 | 0.66±0.19 | 0.71±0.18 | 0.59±0.21 | C vs N,* C vs T † |

VCA indicates VC area; MV, mitral valve; ED, end diastole; and MS, mid systole.
*$P<0.05$; †$P<0.01$; ‡$P<0.001$.

**Table 2. Three-Dimensional Echocardiographic Measurements**

| | Control Subjects (Group C) | HLHS, No Tethering/Prolapse (Group N) | HLHS, Tethered Valve (Group T) | HLHS, Prolapsed Valve (Group P) | *P* |
|---|---|---|---|---|---|
| 3D VC area, $mm^2$ | | 0.20±0.31 | 0.41±0.28 | 0.71±0.29 | N vs P† |
| TV area/BSA at ED, $cm^2/m^2$ | 500±84 | 741±170 | 904±154 | 952±278 | C vs N,‡ C vs T,‡ C vs P‡ |
| Bending angle at ED, degrees | 156.7±9.3 | 160.8±8.2 | 164.8±5.7 | 153.5±7.8 | T vs P* |
| TV area/BSA at MS, $cm^2/m^2$ | 463±122 | 712±146 | 846±105 | 967±240 | C vs N,‡ C vs T,‡ C vs P,‡ N vs P† |
| Bending angle at MS, degrees | 155.4±10.9 | 156.5±12.0 | 164.3±8.5 | 153.2±9.6 | 0.09 |
| Septal leaflet area/TV area ratio | 34.5±5.4 | 16.5±7.2 | 32.5±11.4 | 12.1±6.5 | C vs N,‡ C vs P,‡ N vs T,‡ T vs P‡ |
| AP/LR ratio | 0.98±0.22 | 1.06±0.18 | 1.01±0.23 | 0.99±0.15 | 0.74 |
| Prolapse volume/BSA, $mm^3/m^2$ | 0.01±0.02 | 0.18±0.14 | 0.04±0.06 | 1.10±0.56 | P vs C,‡ P vs N,‡ P vs T‡ |
| Tethered volume/BSA, $mL^3/m^2$ | 0.47±0.22 | 0.29±0.18 | 1.41±0.52 | 0.12±0.09 | T vs C,‡ T vs N,‡ T vs P‡ |
| Prolapse+tethered volume/BSA, $mL^3/m^2$ | 0.49±0.22 | 0.47±0.13 | 1.45±0.51 | 1.22±0.59 | T vs C,‡ T vs N,‡ P vs C,‡ P vs N‡ |
| APM angle, degrees | 93.8±16 | 102.2±8 | 83.9±14.7 | 100.1±7.6 | N vs T† |
| PPM angle, degrees | 82.2±26.7 | 84.8±10.8 | 61.3±12.1 | 77.9±13.8 | C vs T,* N vs T* |

ED indicates end diastole; MS, mid systole; AP, anteroposterior; LR, left-right; APM, anterior PM; and PPM, posterior PM.
*$P<0.05$; †$P<0.01$; ‡$P<0.001$.



classified as group P (prolapse volume >0.46 $mL/m^2$) all had moderate TR. Of the 12 patients classified as group T, 5 had mild TR and 7 had moderate TR.

## Three-Dimensional Echocardiographic Measurements

### *Tricuspid Annular Area*

At both end diastole and mid systole, tricuspid annular area was larger in all HLHS groups compared with control subjects ($P<0.001$; Table 2). In addition, tricuspid annular area was larger in group P compared with group N at mid systole ($P<0.01$).

### *Tricuspid Bending Angle*

The tricuspid bending angle was larger in group T compared with group P at end diastole ($P<0.05$). However, there was no significant difference at mid systole.

### *Ratio of Septal Leaflet Area to TV Annular Area*

This ratio was larger in control subjects compared with groups N and P ($P<0.001$). It also was larger in group T compared with groups P and N ($P<0.001$).

### *Ratio of Combined Prolapse Plus Tethered Volume to BSA*

This ratio was larger in groups T and P compared with group C ($P<0.001$), but there was no difference between group C and N nor between group P and T.

### *PM Angles*

The annular plane and anterior PM maintained an angle of 93.8±16° in control subjects, 102.2±8° in group N, and 100.1±7.6° in group P. However, this angle was 83.9±14.7° in group T, indicating that the anterior PM is tethered more laterally ($P<0.01$, group T versus N). Group T also showed the narrowest angle between the annular plane and the posterior PM compared with groups C and N ($P<0.05$).

## Vertical Geometry of the Tricuspid Annulus

The height of the 4 peak points and the mean height at both end diastole and mid systole are given in Table 3. Group P showed a greater height compared with group T in anterior maximal height/RV, lateral minimal height/RV at mid systole, and all points for mean height at mid systole.

**Table 3. Annular Geometry Assessment by 3D Echocardiography**

| | Control Subjects (Group C) | HLHS, No Tethering/Prolapse (Group N) | HLHS, Tethered Valve (Group T) | HLHS, Prolapsed Valve (Group P) | *P* |
|---|---|---|---|---|---|
| Anterior maximal height/RV length at ED | 0.23±0.09 | 0.17±0.08 | 0.18±0.08 | 0.27±0.05 | N vs P, $P=0.06$ |
| Lateral minimal height/RV length at ED | −0.24±0.11 | −0.25±0.16 | −0.18±0.07 | −0.31±0.07 | 0.15 |
| Posterior maximal height/RV length at ED | 0.25±0.11 | 0.21±0.11 | 0.18±0.06 | 0.24±0.04 | 0.21 |
| Septal minimal height/RV length at ED | −0.24±0.10 | −0.15±0.05 | −0.14±0.08 | −0.22±0.08 | C vs N,* C vs T* |
| Mean height of 4 points at ED | 0.48±0.18 | 0.39±0.18 | 0.35±0.13 | 0.52±0.07 | 0.05 |
| Anterior maximal height/RV length at MS | 0.24±0.1 | 0.20±0.07 | 0.17±0.09 | 0.30±0.06 | T vs P* |
| Lateral minimal height/RV length at MS | −0.30±0.14 | −0.29±0.17 | −0.18±0.11 | −0.38±0.11 | T vs P* |
| Posterior maximal height/RV length at MS | 0.25±0.06 | 0.26±0.18 | 0.17±0.11 | 0.31±0.09 | 0.08 |
| Septal minimal height/RV length at MS | −0.21±0.09 | −0.16±0.10 | −0.16±0.09 | −0.25±0.08 | 0.06 |
| Mean height of 4 points at MS | 0.50±0.16 | 0.45±0.17 | 0.34±0.19 | 0.62±0.14 | T vs P† |

ED indicates end diastole; MS, mid systole.
*$P<0.05$; †$P<0.01$.

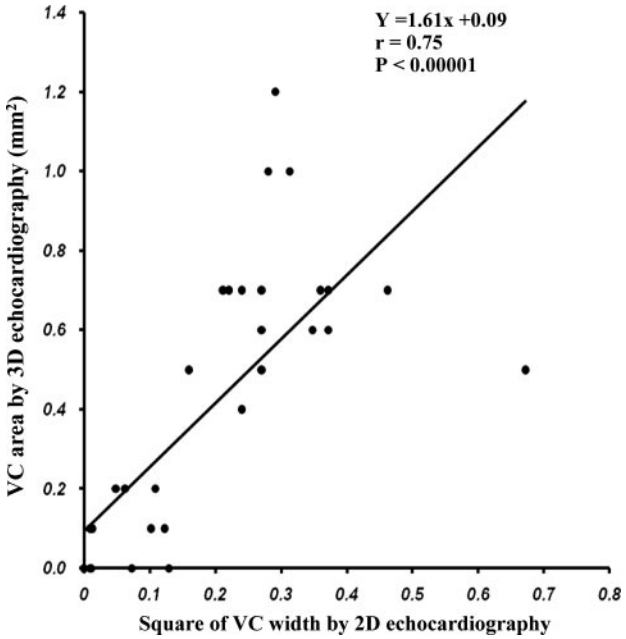


**Figure 6.** Correlation between VC width squared measured by 2D echocardiography and VC area measured by 3D echocardiography.

### Relationship Between 2D and 3D VC Width and Area

There was a strong linear correlation between 2D VC width and the square of the width and 3D VC area ($r$=0.86 and 0.75, respectively; $P$<0.0001; Figure 6). Group P showed a significantly larger 3D VC area compared with group N.

### Factors Influencing Tethering and Prolapse

Factors that separately influenced the ratio of tethering and prolapse volume to BSA were assessed by multiple regression analysis to determine whether the mechanisms might be different from the ratio of combined prolapse and tethered volume to BSA. The following variables were independent predictors of tethered volume (indexed to BSA): lower anterior PM angle ($P$<0.0001) and lower mean height of 4 points at mid systole ($P$=0.008). Independent predictors of prolapse volume (indexed to BSA) were age ($P$=0.001), 3D VC area ($P$=0.024), ratio of TV area at mid systole to BSA ($P$=0.017), and ratio of septal leaflet area to TV area ($P$=0.006).

### Factors Influencing TR VC Area

Independent determinants of TR severity were sphericity index at end diastole, prolapse volume indexed to BSA, and combined tethered and prolapse volume (Table 4).

### Relationship Between LV Size and Degree of TR

There was no relationship between LV size and degree of TR in those patients with significant prolapse or tethering as measured by either LV length or mitral valve annular size. Similarly, there was no correlation between TR VC area as measured by RT3D and LV or mitral valve size.

## Discussion

The major findings in this study are that moderate TR is associated with tethering and prolapse of the TV leaflets in patients with HLHS undergoing surgical palliation. Those with a tethered TV have lateral displacement of their anterior PM, whereas a smaller TV septal leaflet area, annular enlargement, and increasing age are associated with prolapse.

**Table 4. Influence of Parameters on TR (VC Area Measured by RT3D)**

| Parameter | $\beta$ | SE | $P$ |
|---|---|---|---|
| S2/L ratio at ED | 0.39 | 0.19 | 0.048 |
| Prolapse volume/BSA | 0.35 | 0.09 | <0.0001 |
| Tethered+prolapse volume/BSA | 0.20 | 0.07 | 0.006 |

ED indicates end diastole. $R^2$= 0.54.

### Three-Dimensional Analysis Method

At a median of 42 Hz, the frame rates were almost double those from our previous reports.[10,11] This enhances temporal resolution during analysis of the RT3D data sets, particularly in children with higher heart rates. The validity of the software used to analyze the RT3D data sets had previously been tested by our group in a phantom model.[10]

### RV Geometry and Function

The normal tricuspid annulus has 2 high and low points[6,8,11] and, when viewed from a 3-dimensional perspective, has some intrinsic tethering and prolapse. The RV is poorly suited to contract against high afterload[15] and, when faced with a high afterload, assumes a more cylindrical shape, with leftward septal shift resulting in annular dilatation and leaflet tethering.[15–17]

Similar findings were noted in patients with HLHS in whom the annulus changed from a normal elliptical[10] to a more circular shape.[11] It is unlikely that the observed changes in this study are related only to alterations in global function and shape change. It also appears that LV size in HLHS did not appear to affect the degree of TR or to be related to significant tethering or prolapse.

### PM and Leaflet Abnormalities

This study revealed that significant TR is associated with either leaflet tethering or prolapse. Tethering is associated with lateral displacement of the supporting PM, confirming our prior observations.[11] Valve tethering is associated with a more planar annulus as noted by the bending angle, which, in conjunction with PM displacement, increases the pull on the tension apparatus. These findings are similar to observations in adults with functional TV or mitral valve regurgitation.[18–20]

TR secondary to prolapse was associated with greater annular height compared with tethering, suggesting a relationship between supporting apparatus and annular height. In patients with prolapse, PM location was similar to control subjects and HLHS patients with minimal regurgitation, suggesting that either chordal elongation or secondary leaflet abnormalities were the cause. To add to the complexity, the prolapse group also had a smaller septal leaflet. The observation of variability in tricuspid septal leaflet morphology is not new[21]; in this study, however, it appears to be associated with a greater degree of prolapse. This mechanism is understandable because in the normal heart the septal leaflet provides an extensive surface for leaflet coaptation.[22] Of

interest, even those in group N appear to have more intrinsic prolapse than control subjects, although it did not reach statistical significance. Whether this is acquired or a component of the TV at birth in HLHS is unclear.

### Assessment of the Severity of TR

Although our data demonstrated a good correlation between 2D VC area and width with RT3D VC area, this existed only in those patients in whom prolapse was the predominant mechanism. The size of the 2D VC and its relationship to prolapse and or tethering did not stand up to multivariate analysis, but the 3D VC did. This finding is understandable because the trileaflet nature of the TV creates a complex VC geometry that is better assessed in 3 than 2 dimensions.[12,14]

Older age appeared to be associated with a greater degree of prolapse and annular dilatation. Tethering, however, was seen more frequently in younger patients and might suggest a different underlying mechanism of valve failure.

### Potential Underlying Mechanisms of TV Failure

An increase in mass and afterload in the univentricular heart potentially affects the ischemic threshold with resultant myocardial dysfunction.[23,24] These patients are born with a ventricle that has been submitted to a fetal volume overload of ≈230% of normal, which is augmented shortly thereafter in many patients by a shunt procedure to ≈280%.[25] This chronic volume overload has a deleterious effect on the ventricle until the subsequent bidirectional cavopulmonary shunt and Fontan operation.[26] In a manner similar to post–atrial switch patients, the coronary arterial supply of HLHS hearts may be inadequate to meet the needs of an increased myocardial mass.[27] The observation that post-Fontan patients have reduced coronary flow reserve also points to a potential coronary supply-demand mismatch in such patients.[28]

### Clinical Significance of RT3D Findings

The current technique for tricuspid valve repair in HLHS is bicuspidization of the leaflets. Although used extensively, it does not address TR in the vicinity of the anteroseptal commissure, nor does it specifically address leaflet prolapse or tethering. The use of the RT3D technique provides unique information about prolapse and tethering of the TV leaflets, their relationship to supporting PMs, and the sites of TR. This type of information may permit a more tailored approach to TV repair in the future.

### Limitations

Measurements were performed at end diastole and mid systole and thus do not reflect the remainder of the cardiac cycle. We could measure only the size of the septal leaflet because it is difficult to identify the anterior-posterior leaflet commissure while navigating through the "2D" images in the RT3D data set. This study does not address the time frame of the development of TR in patients with HLHS. We used 2D images to assess RV function because at the time of the study this was the acceptable standard by echocardiography.[29] Once well validated and demonstrated to be reproducible, RT3D will most likely become the acceptable standard for RV volumetric assessment. We did not assess the interobserver and intraobserver variabilities of measurement in this study. Multiple statistical comparisons were made with a relatively small sample size, so values of $P>0.001$ should be interpreted with caution.

## Conclusions

This study confirms our previous observations that tricuspid annular dynamics and PM displacement are important associations with significant TR in HLHS. Moreover, it appears that leaflet tethering is associated with PM displacement and significant regurgitation. On the other hand, the combination of significant prolapse without PM displacement and a smaller septal leaflet size appears to be one of the other mechanisms of TV failure.

## Source of Funding

Dr Takahashi's research was supported by a grant from the Stollery Children's Hospital.

## Disclosures

None.

## References

1. Tweddell JS, Hoffman GM, Mussattoe KA, Fedderly RT, Berger S, Jaquiss RD, Ghanayem NS, Frisbee SJ, Litwin SB. Improved survival of patients undergoing palliation of hypoplastic left heart syndrome: lessons learned from 115 consecutive patients. *Circulation*. 2002;106(suppl):I-82–I-89.
2. Ohye RG, Gomez CA, Goldberg CS, Graves HL, Devaney EJ, Bove EL. Tricuspid repair in hypoplastic left heart syndrome. *J Thorac Cardiovasc Surg*. 2004;127:465–472.
3. Reyes A, Bove EL, Mosca RS, Kulik TJ, Ludomirsky A. Tricuspid valve repair in children with hypoplastic left heart syndrome during staged surgical reconstruction. *Circulation*. 1997;96(suppl):341–345.
4. Barber G, Helton G, Aglira BA, Chin AJ, Murphy JD, Rigott JD, Norwood WI. The significance of tricuspid regurgitation in hypoplastic left heart syndrome. *Am Heart J*. 1988;116:1563–1567.
5. Chang AC, Farrell PE, Murdison KA, Baffa JM, Barber G, Norwood WI Murphy JD. Hypoplastic left heart syndrome: hemodynamic and angiographic assessment after initial reconstructive surgery and relevance to modified Fontan procedure. *J Am Coll Cardiol*. 1991;17:1143–1149.
6. Fukuda S, Gillinov AM, McCarthy PM, Stewart WJ, Song JM, Kihara T, Daimon M, Shin MS, Thomas JD, Shiota T. Determinants of recurrent or residual functional tricuspid regurgitation after tricuspid annuloplasty. *Circulation*. 2006;114(suppl I):I-582–I-587.
7. Fukuda S, Song JM, Gillinov, McCarthy PM, Daimon M, Kongsaerepong V, Thomas JD, Shiota T. Tricuspid valve tethering predicts residual tricuspid regurgitation after tricuspid annuloplasty. *Circulation*. 2006;111:975–979.
8. Ton-Nu TT, Levine RA, Handschumasher MD, Dorer DJ, Yosefy C, Fan D, Hua L, Jiang L, Hung J. Geometric determinants of functional tricuspid regurgitation. *Circulation*. 2006;114:143–149.
9. Fukuda S, Saracino G, Matsumura, Daimon M, Tran H, Greenberg NL, Hozumi T, Yoshikawa J, Thomas JD, Shiota T. Three dimensional geometry of the tricuspid annulus in healthy subjects and in patients with functional tricuspid regurgitation. *Circulation*. 2006;114(suppl)I-495–I-498.
10. Nii M, Roman KS, Macgowan CK, Smallhorn JF. Insight into normal mitral and tricuspid annular dynamics in pediatrics: a real-time three-dimensional echocardiographic study. *J Am Soc Echo*. 2005;18:805–814.
11. Nii M, Guerra V, Roman KS, Macgowan CK, Smallhorn JF. Three-dimensional tricuspid annular function provides insight into the mechanisms of tricuspid-valve regurgitation in classic hypoplastic left heart syndrome. echocardiography and computer reconstruction. *J Am Soc Echo*. 2006;19:391–402.
12. Tribouilloy CM, Enriquez-Sarano M, Bailey KR, Tajik AJ, Seward JB. Quantification of TR by measuring the width of the vena contracta with Doppler color flow imaging: a clinical study. *J Am Coll Cardiol*. 2000; 36:472–478.
13. Reynertson SI, Kundur R, Mullen GM, Costanzo MR, McKeinan TL, Louie EK. Asymmetry of right ventricular enlargement in response to tricuspid regurgitation. *Circulation*. 1999;100:465–467.

14. Velayudhan DE, Brown TM, Nanda NC, Patel V, Miller AP, Mehmood F, Rajdev S, Fang L, Frans EE, Vengala S, Madadi P, Yelamanchili P, Baysan O. Quantification of tricuspid regurgitation by live three-dimensional transthoracic echocardiographic measurements of vena contracta area. *Echocardiography*. 2006;23:793–798.
15. Hinderliter AL, Willis PW, Long WA, Clarke WR, Ralph D, Caldwell EJ, Williams W, Ettinger NA, Hill NS, Summer WR, de Boisblanc B, Koch G, Li S, Clayton LM, Jöbsis MM, Crow JW. Frequency and severity of tricuspid regurgitation determined by Doppler echocardiography in primary pulmonary hypertension. *Am J Cardiol*. 2003;91:1033–1037.
16. Sukmawan R, Akasaka T, Watanabe N, Akiyama M, Wada N, Taniguchi M, Kawamoto T, Yoshida K. Quantitative assessment of right ventricular geometric remodeling in pulmonary hypertension secondary to left-sided heart disease using real-time three-dimensional echocardiography. *Am J Cardiol*. 2004;94:1096–1099.
17. Sukmawan R, Watanabe N, Ogasawara Y, Yamaura Y, Yamamoto K, Wada N, Kume T, Okura H, Yoshida K. Geometric changes of tricuspid valve tenting in tricuspid regurgitation secondary to pulmonary hypertension quantified by novel system with transthoracic real-time 3-dimensional echocardiography. *J Am Soc Echocardiogr*. 2007;20:470–476.
18. Fukuda S, Gillinov AM, Song JM, Daimon M, Kongsaerepong V, Thomas JD, Shiota T. Echocardiographic insight into atrial and ventricular mechanisms of functional tricuspid regurgitation. *Am Heart J*. 2006;152:1208–1214.
19. Otsuji Y, Handschumacher MD, Liel-Cohen N, Tanabe H, Jiang L, Schwammenthal E, Guerrero JL, Nicholls LA, Vlahakes GJ, Levine RA. Mechanism of ischemic mitral regurgitation with segmental left ventricular dysfunction: three-dimensional echocardiographic studies in models of acute and chronic progressive regurgitation. *J Am Coll Cardiol*. 2001;37:641–648.
20. Salgo IS, Gorman JH, Gorman RC, Jackson BM, Bowen FW, Plappert T, St John Sutton MG, Edmunds LH Jr. Effect of annular shape on leaflet curvature in reducing mitral leaflet stress. *Circulation*. 2002;106:711–717.
21. Stamm C, Anderson RH, Ho SY. The morphologically tricuspid valve in hypoplastic left heart syndrome. *Eur J Cardiothorac Surg*. 1997;12:587–592.
22. Van Praagh R, Papagiannis J, Grunenfelder J, Bartram U, Martanovic P. Pathologic anatomy of corrected transposition of the great arteries: medical and surgical implications. *Am Heart J*. 1998;135:772–785.
23. Sidi D. Cardiac and pulmonary physiology in the functionally univentricular circulation with reference to the total cavo-pulmonary connection. *Cardiol Young*. 2005:15;26–30.
24. Li W, Hornung TS, Francis DP, O'Sullivan C, Duncan A, Gatzoulis M, Henein M. Relation of biventricular function quantified by stress echocardiography to cardiopulmonary exercise capacity in adults with Mustard procedure for transposition of the great arteries. *Circulation*. 2004;110:1380–1386.
25. Hijazi ZM, Fahey JT, Kleinman CS, Kopt GS, Hellenbrand WE. Hemodynamic evaluation before and after closure of fenestrated Fontan. *Circulation*. 1992;86:196–202.
26. Gewillig M, Daren W, Auberr A, Van dere Hauwaert L. Abolishment of a chronic volume overload: implications for diastolic function of the systemic ventricle immediately after Fontan repair. *Circulation*. 1992;86:93–99.
27. Babu-Narayan S, Goktekin O, Moon JC, Broberg CS, Pantely GA, Pennell DJ, Gatzoulis MA, Kilner PJ. Late gadolinium enhancement cardiovascular magnetic resonance of the systemic right ventricle in adults with previous atrial redirection surgery for transposition of the great arteries. *Circulation*. 2005;111:2091–2098.
28. Hauser M, Bengel FM, Kuhn A, Sauer U, Nekolla SG, Eicken A, Schwaiger M, Hess J. Myocardial perfusion and coronary reserve assessed by positron emission tomography in patients after Fontan-like operations. *Pediatr Cardiol*. 2003;24:386–392.
29. Lang RM, Bierig M, Devereux RB, Flachskampf FA, Foster E, Pellikka PA, Picard MH, Roman MJ, Seward J, Shanewise JS, Solomon SD, Spencer KT, St John Sutton M, Stewart WJ. Recommendation for chamber quantification: a report from the American Society of Echocardiography's Guidelines and Standards Committee and the Chamber Quantification Writing Group, development in conjunction with the European Association of Echocardiography, a branch of the European Society of Cardiology. *J Am Soc Echocardiogr*. 2005;18:1440–1463.

## CLINICAL PERSPECTIVE

Significant tricuspid valve regurgitation is a major risk factor in hypoplastic left heart syndrome. Thus far, our understanding of the mechanisms responsible for tricuspid valve regurgitation is limited. In addition, surgical treatment of tricuspid regurgitation tends to be nonspecific, usually involving bicuspidization of the valve. Real-time 3-dimensional echocardiography may provide insight into the mechanisms of tricuspid valve regurgitation. This technique permits an evaluation of the spatial relationships between the tricuspid annulus, leaflets, and their supporting apparatus. Real-time 3-dimensional color Doppler also permits accurate evaluation of the severity of regurgitation. This cross-sectional study addressed the mechanisms of tricuspid valve regurgitation in a group of 35 patients with hypoplastic left heart syndrome, all of whom were at various stages after first-stage palliation. All had no more than mild regurgitation at the time of initial presentation. Real-time 3-dimensional echocardiography was used to extract spatial coordinates of the tricuspid annulus, leaflets, and supporting papillary muscles. Three-dimensional color Doppler was used to determine the severity of regurgitation. Analysis of the data revealed that moderate tricuspid regurgitation was associated with tethering and prolapse of the leaflets. Those with tethering had lateral displacement of the anterior papillary muscle and a more planar tricuspid annulus. On the other hand, prolapse was associated with a smaller septal leaflet area, older age, and annular dilatation. This study allows an improved understanding of the mechanisms of tricuspid valve regurgitation in hypoplastic left heart syndrome, with the potential to assist surgeons in targeting specific mechanisms.

# Real-Time 3-Dimensional Echocardiography Provides New Insight Into Mechanisms of Tricuspid Valve Regurgitation in Patients With Hypoplastic Left Heart Syndrome

K. Takahashi, A. Inage, I.M. Rebeyka, D.B. Ross, R.B. Thompson, A.S. Mackie and J.F. Smallhorn

*Circulation.* 2009;120:1091-1098; originally published online September 8, 2009;
doi: 10.1161/CIRCULATIONAHA.108.809566
*Circulation* is published by the American Heart Association, 7272 Greenville Avenue, Dallas, TX 75231

Print ISSN: 0009-7322. Online ISSN: 1524-4539